

# Design of a highly-birefringent microstructured photonic crystal fiber for pressure monitoring

Charles M. Jewart,<sup>1</sup> Sully Mejía Quintero,<sup>2</sup> Arthur M. B. Braga,<sup>2</sup> and Kevin P. Chen<sup>1,\*</sup>

<sup>1</sup>Department of Electrical and Computer Engineering, University of Pittsburgh, Pittsburgh, PA 15261, USA

<sup>2</sup>Departamento de Engenharia Mecânica, Pontifícia Universidade Católica, Rio de Janeiro, RJ, Brazil  
[\\*pec9@pitt.edu](mailto:*pec9@pitt.edu)

**Abstract:** We present the design of an air hole microstructured photonic crystal fiber for pressure sensing applications. The air-hole photonic crystal lattices were designed to produce a large intrinsic birefringence of  $1.16 \times 10^{-3}$ . The impact of the surrounding air holes for pressure sensing to the propagation mode profiles and indices were studied and improved, which ensures single mode propagation in the fiber core defined by the photonic crystal lattice. An air hole matrix and a practical chemical etching process during the fiber preparation stage is proposed to produce an optical fiber with a birefringence-pressure coefficient of  $43.89 \times 10^{-6} \text{MPa}^{-1}$  or a fiber Bragg grating pressure responsivity of 44.15 pm/MPa, which is a 17 times improvement over previous photonic crystal fiber designs.

©2010 Optical Society of America

**OCIS codes:** (060.2280) Fiber design and fabrication, (060.2370) Fiber optics sensors, (060.4005) Microstructured fibers, (060.5295) Photonic crystal fibers, (000.4430) Numerical approximation and analysis.

---

## References and Links

1. T. Nasilowski, T. Martynkien, G. Statkiewicz, M. Szpulak, J. Olszewski, G. Golojuch, W. Urbanczyk, J. Wojcik, P. Mergo, M. Makara, F. Berghmans, and H. Thienpont, "Temperature and pressure sensitivities of the highly birefringent photonic crystal fiber with core asymmetry," *Appl. Phys. B* **81**(2-3), 325–331 (2005).
2. M. Szpulak, T. Martynkien, and W. Urbanczyk, "Effects of hydrostatic pressure on phase and group modal birefringence in microstructured holey fibers," *Appl. Opt.* **43**(24), 4739–4744 (2004).
3. M. Szpulak, G. Statkiewicz, J. Olszewski, T. Martynkien, W. Urbanczyk, J. Wójcik, M. Makara, J. Klimek, T. Nasilowski, F. Berghmans, and H. Thienpont, "Experimental and theoretical investigations of birefringent holey fibers with a triple defect," *Appl. Opt.* **44**(13), 2652–2658 (2005).
4. M. Antkowiak, R. Kotynski, T. Nasilowski, P. Lesiak, J. Wojcik, W. Urbanczyk, F. Berghmans, and H. Thienpont, "Phase and group modal birefringence of triple-defect photonic crystal fibres," *J. Opt. A, Pure Appl. Opt.* **7**(12), 763–766 (2005).
5. S. Barkou Libori, J. Broeng, E. Knudsen, A. Bjarklev, and H. R. Simonsen, "High-birefringent photonic crystal fiber," *OFC 2001. Optical Fiber Communication Conference and Exhibit. Technical Digest Postconference Edition*. (IEEE, 2001) pp. TuM2-1-3
6. NKT Photonics - Photonic Crystal Fibers, SuperK Continuum Laser, Koheras Fiber Lasers, <http://www.blazephotonics.com>
7. H. K. Gahir, and D. Khanna, "Design and development of a temperature-compensated fiber optic polarimetric pressure sensor based on photonic crystal fiber at 1550 nm," *Appl. Opt.* **46**(8), 1184–1189 (2007).
8. H. Y. Tam, S. K. Khijwania, and X. Y. Dong, "Temperature-Insensitive Pressure Sensor using a Polarization-Maintaining Photonic Crystal Fiber based Sagnac Interferometer," *2007 Asia Optical Fiber Communication and Optoelectronics Conference*, (IEEE, 2007) pp. 345-347.
9. F. C. Fávero, S. M. M. Quintero, V. V. Silva, C. Martelli, A. M. B. Braga, I. C. S. Carvalho, and R. W. A. Llerena, "Photonic crystal fiber pressure sensor," *Proc. SPIE* **7503**, 750364 (2009).
10. M. Szpulak, T. Martynkien, and W. Urbanczyk, "Highly birefringent photonic crystal fibre with enhanced sensitivity to hydrostatic pressure," 2006 International Conference on Transparent Optical Networks, (ICTON, 2006) pp. 174-177.
11. T. Martynkien, G. Statkiewicz-Barabach, J. Olszewski, J. Wojcik, P. Mergo, T. Geernaert, C. Sonnenfeld, A. Anuszkiewicz, M. K. Szczerkowski, K. Tarnowski, M. Makara, K. Skorupski, J. Klimek, K. Poturaj, W. Urbanczyk, T. Nasilowski, F. Berghmans, and H. Thienpont, "Highly birefringent microstructured fibers with enhanced sensitivity to hydrostatic pressure," *Opt. Express* **18**(14), 15113–15121 (2010).
12. S. Kim, C. S. Kee, and C. G. Lee, "Modified rectangular lattice photonic crystal fibers with high birefringence and negative dispersion," *Opt. Express* **17**(10), 7952–7957 (2009).
13. C. Martelli, J. Canning, N. Groothoff, and K. Lyytikäinen, "Strain and temperature characterization of photonic crystal fiber Bragg gratings," *Opt. Lett.* **30**(14), 1785–1787 (2005).

14. R. Ghosh, A. Kumar, J. P. Meunier, and E. Marin, "Modal characteristics of few-mode silica-based photonic crystal fibres," *Opt. Quantum Electron.* **32**(6/8), 963–970 (2000).
  15. C. Jewart, and D. Xu, "J. Canning and K. P. Chen, "Structure optimization of air-hole fibers for high-sensitivity fiber Bragg grating pressure sensors," *Proc. SPIE* **7004**, 70041Z (2008).
  16. S. Kreger, S. Calvert, and E. Udd, "High Pressure Sensing Using Fiber Bragg Gratings Written into Birefringent Side Hole Fiber," *2002 15th Optical Fiber Sensors Conference Technical Digest*. (IEEE, 2002), pp. 355-358.
  17. J. R. Clowes, S. Syngellakis, and M. N. Zervas, "Pressure Sensitivity of Side-Hole Optical Fibers," *IEEE Photon. Technol. Lett.* **10**(6), 857–859 (1998).
  18. I. H. Malitson, "Interspecimen Comparison of the Refractive Index of Fused Silica," *J. Opt. Soc. Am.* **55**(10), 1205–1209 (1965).
  19. W. Urbanczyk, T. Martynkien, and W. J. Bock, "Dispersion effects in elliptical-core highly birefringent fibers," *Appl. Opt.* **40**(12), 1911–1920 (2001).
  20. J. Noda, K. Okamoto, and Y. Sasaki, "Polarization maintaining fibers and their applications," *J. Lightwave Technol.* **4**(8), 1071–1089 (1986).
- 

## 1. Introduction

Fiber sensors based on air-hole microstructured fibers have received considerable attention recently for their versatility in tuning mechanical, thermal, and optical properties through the design of the fiber. This flexibility has enabled the fabrication of many new and exciting fibers with unique properties that are unattainable in conventional fibers. For example, in many fiber sensing applications, polarization maintaining (PM) fibers are desired because they provide a better signal-to-noise ratio and allow for simplification of the measurements. Using air-hole microstructured designs, PM fibers with birefringences in excess of  $1 \times 10^{-3}$  [1–5] can be readily manufactured, which is more than an order of magnitude than that of conventional fibers.

Given the importance of PM fibers, a number of air-hole fiber designs have been proposed and studied. PM fibers derived from Panda fiber with a hexagonal air-hole lattice have become commercially available [6]. Fiber sensors based on these types of fibers have been extensively reported.

A review of prior research on photonic crystal fiber (PCF) design and sensor implementation shows that the research focus was placed on the design of an air-hole lattice to achieve a high birefringence. Their suitability for sensing applications was not a priority during the design of the fiber. Due to this reason, fiber sensors using commercially available polarization maintaining photonic crystal fibers (PM-PCF) have lower sensitivities than those using conventional fibers. For example, pressure sensors using PM-PCF [7–9] have 5.44 times lower birefringence-pressure sensitivities than that of two-hole solid-core optical fibers. Thus, some research efforts were devoted to design PM-PCF with better pressure sensitivity [10,11].

In this paper, we present the design and numerical simulation of a PM-PCF to achieve the best possible pressure sensitivity. Simultaneously, we considered the optical properties of the air-hole PCF matrix to achieve an initial high birefringence and side hole array to maximize the sensor's sensitivity.

## 2. PCF fiber design

The fiber was designed to be in single-mode operation at 1550 nm and at the same time to have large intrinsic birefringence. The air-hole matrix design is based on a square lattice, which can be modified to exhibit large birefringence [12]. The air hole matrix has a  $1.34 \mu\text{m}$  pitch ( $\Lambda$ ) and  $0.66 \mu\text{m}$  hole diameter ( $d$ ), respectively based on an existing PCF design [13]. These values led to an effective cladding index of 1.4 [14]. To form a fiber core, a single air hole in the middle row was taken out to create the fiber core. The asymmetry was introduced by displacing the central row of air holes on both sides of the fiber core by  $0.46 \mu\text{m}$ . This displacement value was determined from the V-number calculation [14] that a core radius of  $1.9 \mu\text{m}$  was the largest possible size to retain single-mode operation. All dimensions were measured from the center of the fiber core to the center of the adjacent air hole. This resulted in the core having radii of  $1.99 \mu\text{m}$  and  $1.34 \mu\text{m}$  along the x and y axis, respectively. This photonic crystal lattice design ensures single mode operation at 1550 nm with an intrinsic

birefringence of  $8.04 \times 10^{-4}$ , this is obtained by the finite element analysis using COMSOL package using 3 rows of air holes above and below the fiber core.

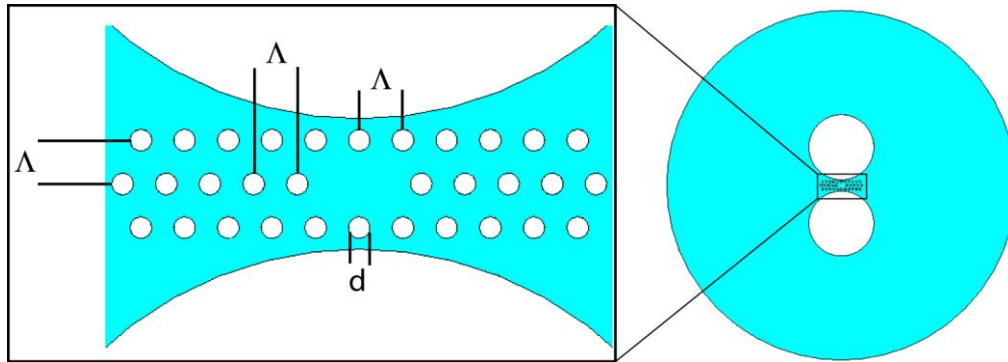


Fig. 1. Schematic design of PCF matrix.

To measure an applied hydrostatic load using fiber grating sensors, large air holes should be introduced into the fiber cladding [15–17]. Previous studies have shown [15] that improved sensitivity can be achieved by placing the fiber core close to the air holes. To ensure optimized pressure sensitivity, the air-hole photonic crystal lattice was placed in a close proximity of the large air holes with only one row of the air hole lattice separated between the fiber core and large hole as shown in Fig. 1. The introduction of large air holes reduces the cladding index, therefore, ensuring optical confinement using only one row of air hole above and below fiber core.

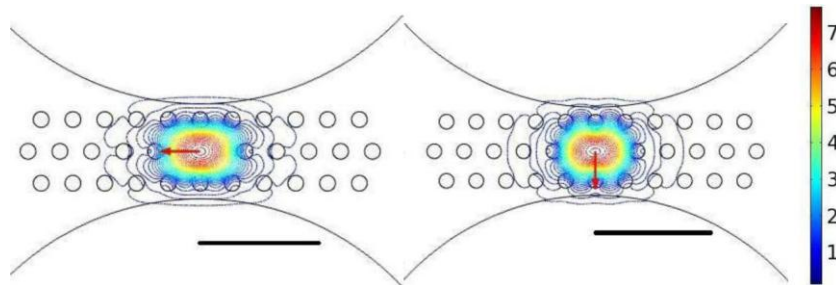


Fig. 2. Electric field distribution of the fundamental mode for x (left) and y (right) polarizations, the black scale bar in the figure indicate  $5 \mu\text{m}$ . The color scale bar indicates relative intensity of guided mode electric fields.

Figure 2 shows the electrical field distribution of the fundamental mode for x and y polarization with the air hole radius of  $11.629 \mu\text{m}$ . The distance between the edges of the large air hole to the center of the upper row of air hole matrix is  $0.66 \mu\text{m}$ . The index of refraction of silica was calculated using the three-term Sellmeier polynomial [18] where it was assumed to have a refractive index of  $n = 1.44504$  at  $1550 \text{ nm}$ , while the air-holes had a refractive index of  $n = 1$ . The resulting initial birefringence for the two-hole PCF with the asymmetric core at  $1550 \text{ nm}$  is  $1.16 \times 10^{-3}$ . The electric field distributions of the fundamental mode for the x ( $n_x = 1.406739$ ) and y ( $n_y = 1.405579$ ) polarizations are presented in Fig. 2. The introduction of two air holes actually increases the birefringence to  $1.16 \times 10^{-3}$ , which is 1.44 times larger than the fiber core that used three rows of air holes for the optical confinement.

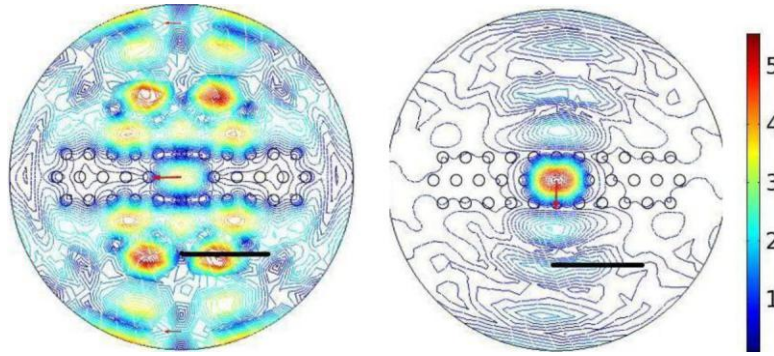


Fig. 3. Electric field distribution of the fundamental mode for x (left) and y (right) polarizations for single-row PCF matrix in the center region of the fiber, the black scale bar indicates 5  $\mu\text{m}$ . The color scale bar indicates relative intensity of guided mode electric fields.

Numerical simulation also reveals that the air hole lattice cannot support a well confined single mode if only one or two rows of air holes were used above and below the fiber core, due to reduced index contrast between the fiber core and the effective cladding index. This is confirmed in Fig. 3 for the case of one row of air holes.

Given the fact that one row of air holes above and below the fiber core cannot confine guided modes, the replacement of the additional rows of air holes by a pair of single large air holes will have a significant impact on the fiber core's optical confinement. Therefore, the overall radius of the single large air hole was studied to observe how the air hole radius effects modal confinement. To observe the dependency of the radius of curvature of the air-hole, the radius of the round holes were increased while maintaining the spacing between the PCF matrix and the edge of the air-hole in order. The effective index for the two eigen-modes ( $n_x$  and  $n_y$ ) for the fundamental mode are presented in Fig. 4a.

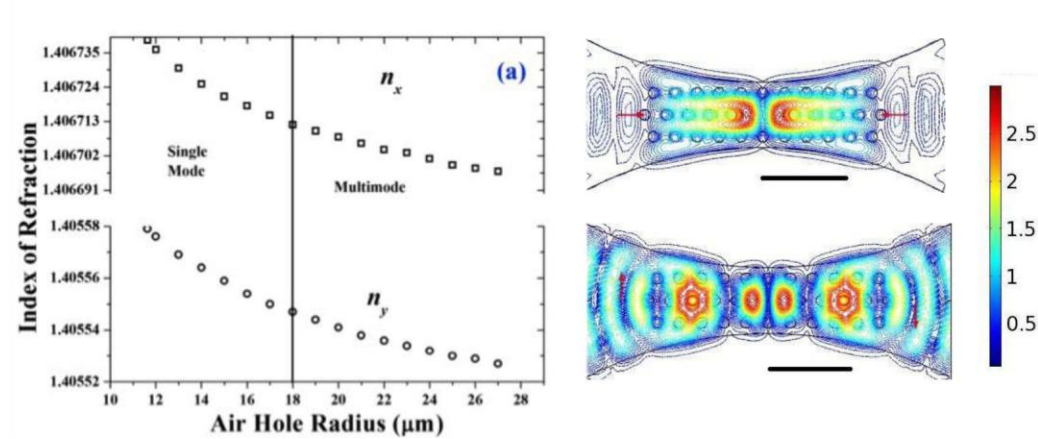


Fig. 4. (a) Effective index of refraction for  $n_x$  (top) and  $n_y$  (bottom) vs hole radius and (b) higher order mode profiles with air hole radius of 24  $\mu\text{m}$ . The color scale bar indicates relative intensity of guided mode electric fields.

As the radius of curvature for the air-hole increases the indices of refraction for the two polarization modes decrease exponentially. The fiber remains in single mode operation up to an air-hole radius of 19  $\mu\text{m}$ , at this limit, higher order modes begin to appear. The fiber that possessed the large air-hole with a radius of 11.629  $\mu\text{m}$  possessed effective indices of refraction of 1.406739 and 1.405579 for the two orthogonal polarized modes, respectively, which results in a birefringence of  $1.160 \times 10^{-3}$ . The fiber birefringence changes to  $1.165 \times 10^{-3}$  when the radius of air hole increases to 18  $\mu\text{m}$ .

Although the indices of refraction for both polarizations and the birefringence of guided modes are only moderately affected by the change in the air hole sizes, modal confinement is heavily influenced by the radius of the large air hole. Higher order modes are produced when the air hole radius goes beyond 19  $\mu\text{m}$ , which is due to the reduction in effective index of the cladding due to the increased size of air holes. Figure 4b presented guided mode profiles for both x- and y- polarization with the air hole radius of 24  $\mu\text{m}$ . The trend of the fiber to shift into multimode operation with an increasing air-hole radius also eliminates the possibility to use a pair of large air-hole to effectively transfer the hydrostatic load to the core region as demonstrated with the fiber with a conventional fiber core made of Ge-doped silica [15–17].

### 3. Fiber optimization for hydrostatic pressure sensing

When a microstructured optical fiber is placed under an applied transverse load such as a hydrostatic pressure, the air-holes in the fiber cladding deform and transfer the induced stress into the central core region. The resulting stress induces a birefringence that is governed by the following equations

$$\begin{aligned} n_x &= n_0 + C_1\sigma_x + C_2(\sigma_y + \sigma_z) \\ n_y &= n_0 + C_1\sigma_y + C_2(\sigma_x + \sigma_z) \end{aligned} \quad (1)$$

where  $n_x$  and  $n_y$  are index of refractive for two linear polarization,  $C_1$  and  $C_2$  are the stress optic coefficients with values of  $-6.9 \times 10^{-13} \text{ m}^2/\text{N}$  and  $-41.9 \times 10^{-13} \text{ m}^2/\text{N}$ , respectively and  $\sigma_x$ ,  $\sigma_y$ ,  $\sigma_z$  are the principal components of the induced stress. Only the first two components of the index change are needed due to a two-dimensional reduction of the model via plane-strain assumptions. The pressure sensitivity of the phase modal birefringence is determined by the difference between the loaded and unloaded birefringence with respect to the applied load:

$$\frac{dB}{dP} = \frac{B_{\text{Loaded}} - B_{\text{unloaded}}}{P}, \quad (2)$$

The phase and group modal birefringence are two important parameters that are used to characterize birefringence in optical fibers. The phase modal birefringence is defined by the difference between  $n_x$  and  $n_y$

$$B = \Delta n = n_x - n_y, \quad (3)$$

corresponding to the slow and fast axis, respectively. The group birefringence,  $G(\lambda)$  is defined as

$$G = B - \lambda \frac{dB}{d\lambda}, \quad (4)$$

Where  $dB/d\lambda$  is the chromatic dispersion of the phase modal birefringence

The phase modal birefringence as a function of wavelength (1.0  $\mu\text{m}$ -1.6  $\mu\text{m}$ ) for an unloaded fiber was calculated for the asymmetric core design. The discrete values of  $B(\lambda)$  were numerically adjusted with a second-degree polynomial, allowing for the calculation of the dispersion term  $dB/d\lambda$  and determination of  $G(\lambda)$ . The phase and group modal birefringence are plotted versus wavelength for the initial design at base pressure and the initial design, small circle design and the etched design for an applied hydrostatic pressure of 20 MPa in Fig. 5.

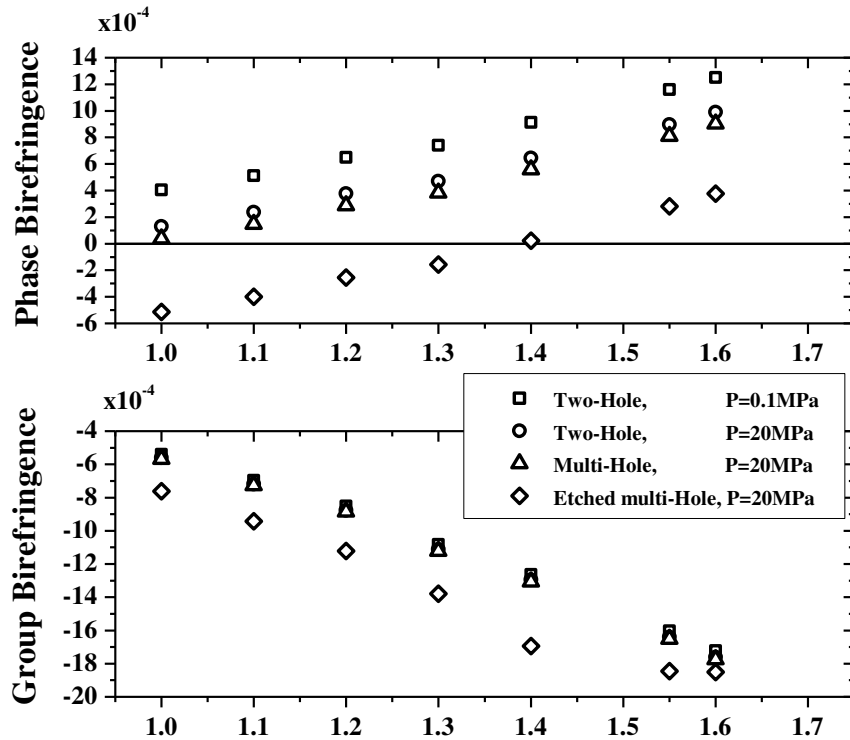


Fig. 5. Wavelength dependence of the phase and group modal birefringence

In the selected coordinate system the phase modal birefringence ( $B$ ) is positive, whereas the group modal birefringence ( $G$ ) is negative. The difference in sign between the phase and group birefringence is caused by a highly anomalous chromatic dispersion in the phase modal birefringence ( $dB/d\lambda > 0$ ). This is different than what occurs in traditional highly birefringent fibers where the chromatic dispersion ( $dB/d\lambda$ ) is significantly smaller [19,20].

Figure 5 also simulates the fiber sensitivity to external pressure. Under an external hydrostatic pressure of 20 MPa, the two-hole fiber with the PCF core incurs a birefringence to pressure sensitivity of  $0.1317 \times 10^{-4}/\text{MPa}$ , if a fiber Bragg grating (FBG) sensor is inscribed in the fiber, this pressure sensitivity will lead to  $\sim 13.34 \text{ pm}/\text{MPa}$ . This is 11% less than the previous report using larger air hole solid core fiber ( $\sim 14.79 \text{ pm}/\text{MPa}$ ) [15]. This is not a surprise due to the smaller air holes used as pressure transducers. As revealed in the simulation, the further increase of the air holes will induce multi-transverse modes, which is not desired for sensing applications.

To increase the sensitivity of the fiber while maintaining single-mode operation for the PCF fiber core, a row of smaller air holes are added to the cladding, which extends from the out-edge of the  $30 \mu\text{m}$  air hole to the edge of the fiber as shown in Fig. 6. This row of air holes has diameters of  $5.68 \mu\text{m}$  and  $0.5 \mu\text{m}$  spacing, which is manufacturable in the fiber perform preparation stage. The addition of air holes has no impact on the single-mode operation of the PCF core, while increasing the compressive stress in the x-polarization in the core region. It is also possible to increase the fiber sensitivity by etching away the silica bridge between two adjacent air holes using a buffered oxide etching (BOE) process [15]. This can be accomplished in the fiber perform before the drawing process, with the core region being able to be sealed from the BOE process. The etching process will remove the silica bridges by etching an amount of the small air holes as shown in Fig. 4b, which improves the pressure transduction into the core region.

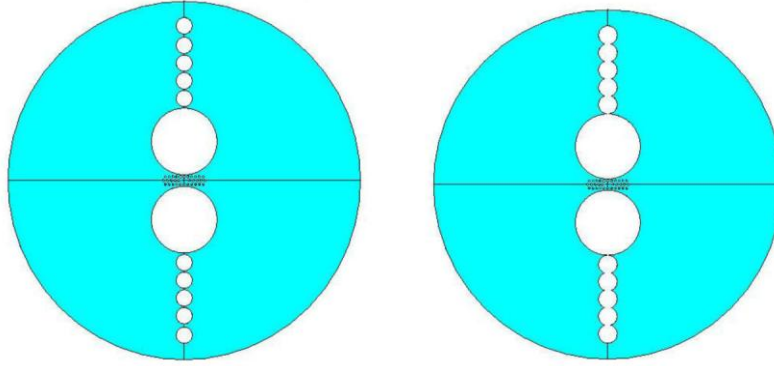


Fig. 6. Multi-hole fiber geometry (left), etched fiber geometry (right)

Figure 7 presents the finite element analysis (FEA) stress analysis of the air-hole fibers before and after etching along x-axis, which is the dominant stress component. The etching process leads to significant increase of compressive stress along x-axis in the core region. The average compressive stress over the entire PCF core region is increased by 2.55 times (from -119.947 to -304.328 at 20 MPa).

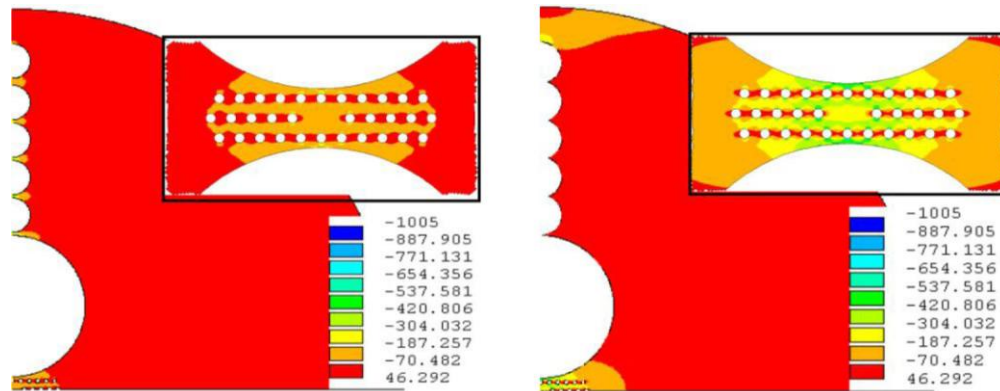


Fig. 7. Stress profile for x-component of stress for the Multi-hole Fiber before (left) and after (right) chemical etching, the color bar has unit of MPa

The FEA analysis also confirms the significant increase of birefringence pressure sensitivity. The addition of one row of air hole with removed silica bridges induce over  $1 \times 10^{-3}$  phase birefringence under 20 MPa hydrostatic pressure as shown in Fig. 5. Figure 8 presents the phase modal birefringence as function of the pressure for two-hole PCF (11.6  $\mu\text{m}$  diameter air hole), two-hole PCF with addition of air-holes before and after the BOE process. Etching the air holes in the cladding results in a birefringence-pressure coefficient and FBG pressure responsivity of  $43.89 \times 10^{-6} \text{MPa}^{-1}$  and 44.15 pm/MPa, respectively, a 3 times improvement over the multi-hole fiber and a 17 times improvement over what has previously been demonstrated in PM-PCFs [1,2,7–9] and more than four times better than the recent results in the Hi-Bi microstructured fiber [11].

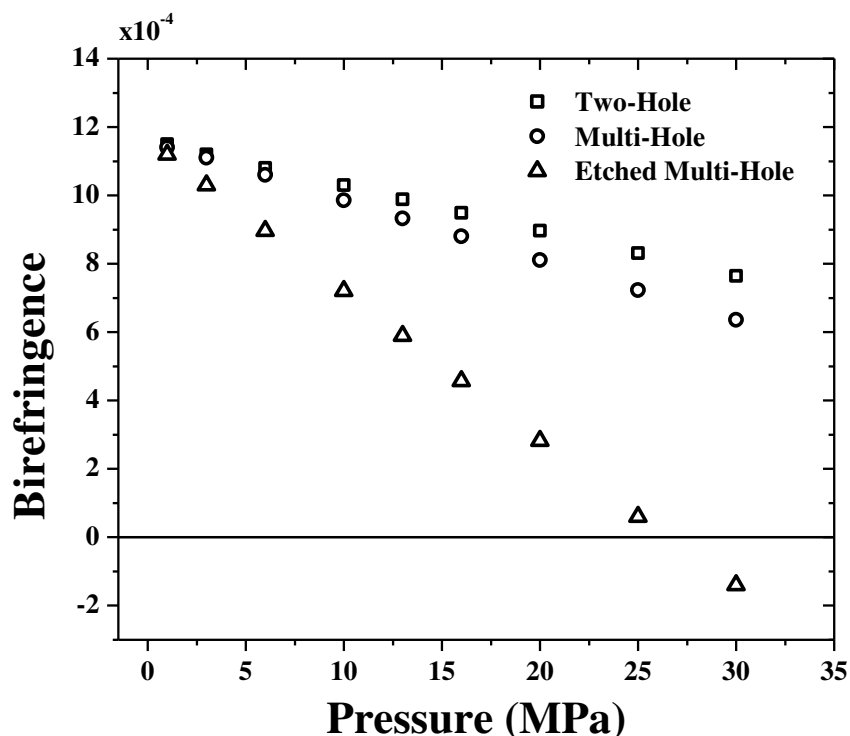


Fig. 8. Pressure sensitivity of phase modal birefringence

#### 4. Summary and conclusion

In Summary, this paper presents numeric studies of side-hole fiber with a highly birefringent PCF core. It shows that the introduction of large air holes in the fiber cladding for sensing applications has a significant impact on the optical properties of the PCF fiber core. Special considerations have been given during the fiber design to ensure single-mode operation with good modal confinement. At the same time, the configuration of the air holes in the fiber cladding also influence the sensitivity of the fiber sensor. Both facts have to be considered simultaneously to achieve an initial high birefringence and side hole array to maximize the sensor's sensitivity.

In this paper, we presented an air hole matrix in the fiber cladding and a practical chemical etching process during the fiber perform preparation stage to produce a highly birefringent photonic crystal fiber with a birefringence-pressure coefficient of  $43.89 \times 10^{-6} \text{MPa}^{-1}$  or a FBG pressure responsivity of 44.15 pm/MPa.

#### Acknowledgements

This work was supported by a National Science Foundation career program (NSF0644681), C. M. Jewart is supported by a NSF IGERT Program with the Mascaro Center for Sustainable Innovation (NSF0504345). Kevin P. Chen's e-mail address is pec9@pitt.edu. C. M. Jewart and S. M. Quintero contributed equally to this work.